Inorganic Chemistry

Article

pubs.acs.org/IC

Photoinduced Electron Transfer in Linear Triarylamine–Photosensitizer–Anthraquinone Triads with Ruthenium(II), Osmium(II), and Iridium(III)

Jihane Hankache,[†] Marja Niemi,[‡] Helge Lemmetyinen,*[,‡] and Oliver S. Wenger*[,†]

[†]Georg-August-Universität Göttingen, Institut für Anorganische Chemie, Tammannstrasse 4, D-37077 Göttingen, Germany

[‡]Tampere University of Technology, Department of Chemistry and Bioengineering, P.O. Box 541, FIN-33101 Tampere, Finland

ABSTRACT: A rigid rod-like organic molecular ensemble comprised of a triarylamine electron donor, a 2,2′-bipyridine (bpy) ligand, and a 9,10-anthraquinone acceptor was synthesized and reacted with suitable metal precursors to yield triads with $Ru(bpy)_3^{2+}$, $Os(bpy)_3^{2+}$, and $[Ir(2\text{-}(p\text{-tolyl})pyridine)_2(bpy)]^+$ photosensitizers. Photoexcitation of these triads leads to long-lived charge-separated states (τ = 80–1300 ns) containing a triarylamine cation and an anthraquinone anion, as observed by transient absorption spectroscopy. From a combined electrochemical and optical spectroscopic study, the thermodynamics and kinetics for the individual photoinduced charge-separation and thermal charge-recombination events were determined; in some cases, measurements on suitable donor–sensitizer or sensitizer–acceptor dyads were necessary. In the case of the ruthenium and iridium triads, the fully charge-separated state is formed in nearly quantitative yield.

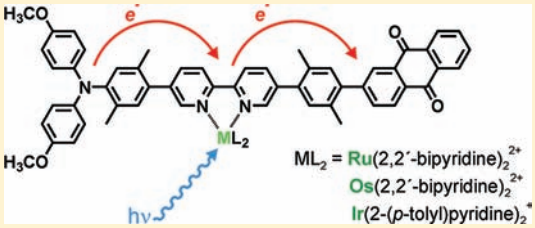

INTRODUCTION

The construction of molecular triads with linear alignment of an electron donor, photosensitizer, and an electron acceptor is of long-standing interest.[1] A key advantage of *linear* rigid rod-like constructs is a maximum separation distance of the electron–hole pair in the charge-separated state. The traditional approach to obtaining linear triads for vectorial electron transfer with d^6 metal photosensitizers involves the use of 2,2′;6′,2″-terpyridine (tpy) ligands, which are substituted at the 4′-position of the central pyridine ring with appropriate electron donors or acceptors (Scheme 1a).[2−10]

However, the $Ru(tpy)_2^{2+}$ photosensitizer has rather poor photophysical properties when compared to $Ru(bpy)_3^{2+}$ (bpy = 2,2′-bipyridine); particularly its short ^{3}MLCT (metal-to-ligand charge transfer) lifetime is less than optimal for photoinduced electron transfer chemistry.[11] Despite the need for shorter excitation wavelengths, isoelectronic $Ir(tpy)_2^{3+}$ complexes represent an attractive alternative from a photophysical point of view, but they are not at all easy to synthesize.[8,12,13] An interesting, newly discovered alternative option is the bis-(diquinolinyl)pyridine ligand, which is structurally similar to tpy (Scheme 1b) but ligates to ruthenium(II) with a significantly larger bite angle, which in turn results in more favorable photophysical properties of the complex.[14−17] Numerous molecular electron transfer triads based on the $Ru(bpy)_3^{2+}$ photosensitizer have been explored. However, when substituting one bpy ligand with an electron donor while equipping a second bpy ligand with an electron acceptor (Scheme 1c), one is often confronted with the problem of isomerism, and analysis of the electron transfer kinetics may become tricky.[18−28] Moreover, the resulting molecular constructs are not linear. A viable solution to this problem is to attach the donor and the acceptor at the 5- and 5′-positions of a given bpy ligand (Scheme 1d). We recently communicated preliminary results on what we believe to be the first rigid rod-like (linear) triad based on the $Ru(bpy)_3^{2+}$ photosensitizer.[29] Here, we present a more detailed study including transient absorption data at higher temporal resolution and an extension of the work to analogous triads with $Os(bpy)_3^{2+}$ and a cyclometalated iridium(III) complex as photosensitizing units. Specifically, we synthesized and investigated the three triads from Scheme 2 along with a series of suitable molecular dyads.

Scheme 1. Possible Constructs of Molecular Triads Incorporating d^6 Metal Complexes (Here, Ru(II)) as Photosensitizers between Electron Donors (D) and Electron Acceptors (A)

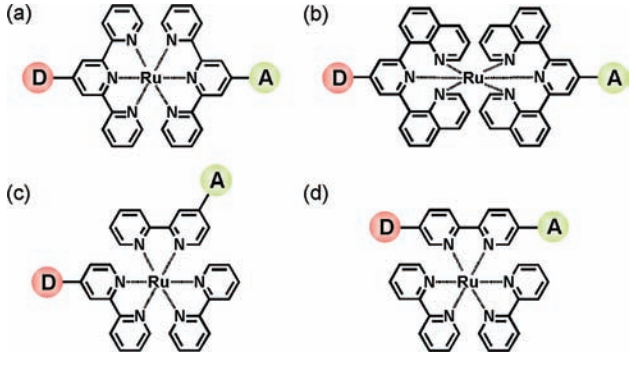

Received: March 15, 2012
Published: May 23, 2012

Scheme 2. The Molecules Investigated in This Work[a]

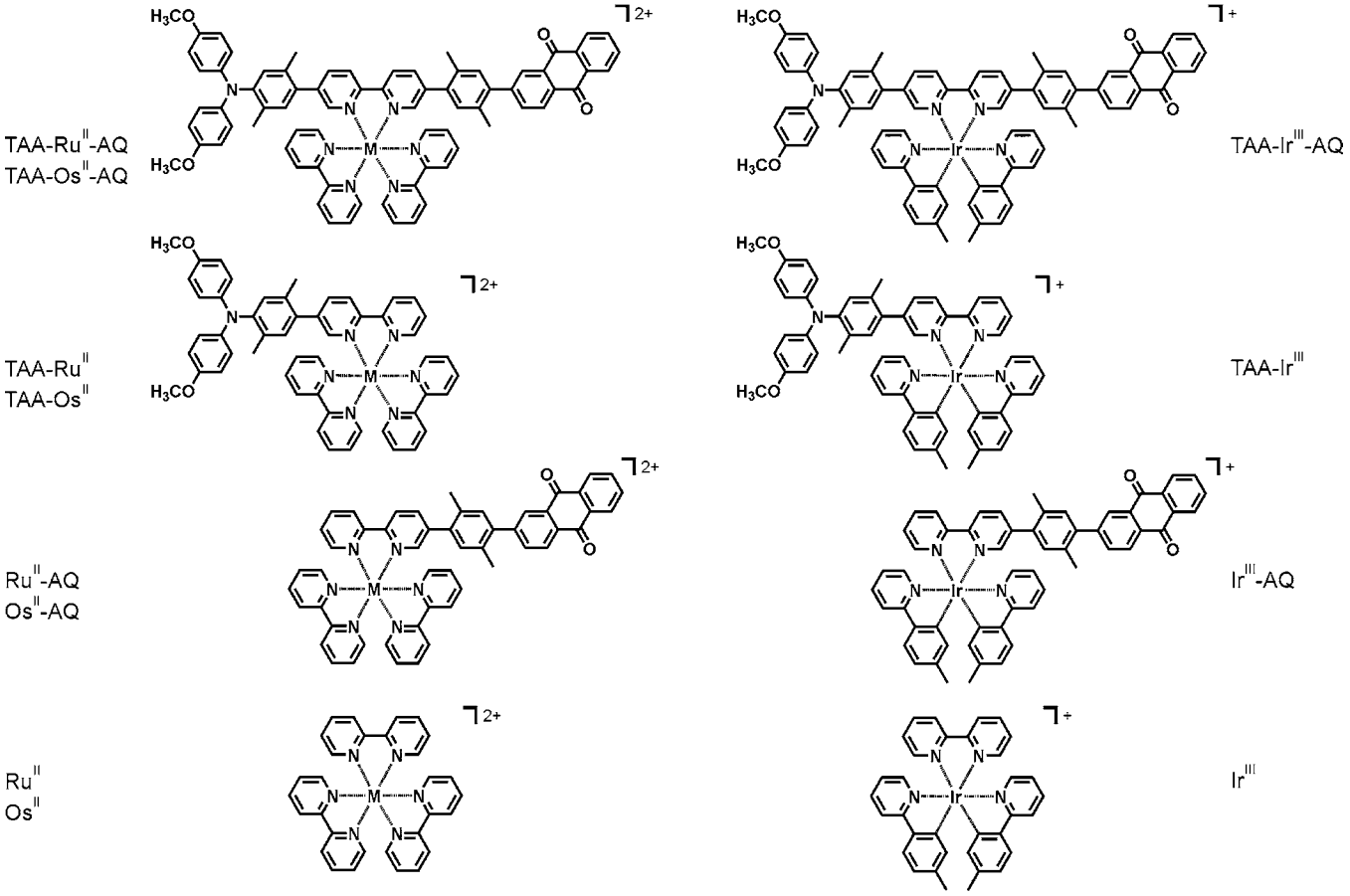

[a]TAA = triarylamine; AQ = anthraquinone.

The triads are comprised of a triarylamine (TAA) electron donor, a d^6 metal diimine photosensitizer (Ru^{II}, Os^{II}, Ir^{III}), and a 9,10-anthraquinone (AQ) unit, which is acting as a terminal electron acceptor. The dyads contain either only the donor and the sensitizer or the sensitizer and the acceptor.

RESULTS AND DISCUSSION

Synthesis. The synthesis of the rigid rod-like triarylamine−2,2′-bipyridine−anthraquinone unit was described in detail in our prior communication.[29] Briefly, the synthetic strategy is based on 5,5′-dibromo-2,2′-bipyridine as a starting material to which 4-(trimethylsilyl)phenylboronic acid was attached on both sides in a Suzuki cross-coupling reaction. After trimethylsilyl-halogen exchange, the resulting molecule can be coupled to anthraquinone-2-boronic acid pinacol ester in a Suzuki-type cross-coupling reaction. A subsequent palladium(0)-catalyzed N−C coupling reaction with 4,4′-dimethoxydiphenylamine then yields the desired molecular rod in 33% overall yield. The syntheses of the dyads departed from 5-bromo-2,2′-bipyridine and relied on the same coupling strategy involving 4-(trimethylsilyl)phenylboronic acid as a first coupling partner, trimethylsilyl-halogen exchange, followed by a reaction either with anthraquinone-2-boronic acid pinacol ester or with 4,4′-dimethoxydiphenylamine. Detailed synthetic protocols can be found in the Supporting Information of our prior communication.[29] Complexation of the dyad and triad ligands to $Ru(bpy)_2Cl_2$, $Os(bpy)_2Cl_2$, and $[Ir(2\text{-}(p\text{-tolyl})\text{-pyridine})_2Cl]_2$[30,31] occurred following standard protocols.[32] Product characterization data are given in the Experimental Section.

Optical Absorption and Luminescence Spectroscopy. Figure 1 shows optical absorption spectra of the individual compounds from Scheme 2 in acetonitrile solution at room-temperature. The ruthenium complexes from panel (a) exhibit metal-to-ligand charge transfer (MLCT) absorption bands centered around 450 nm and a bpy-localized $\pi-\pi^*$ absorption band at 290 nm. The AQ unit has relatively low-lying absorptions, which account for some of the additional extinction observable between 310 and 380 nm in the TAA−Ru^{II}−AQ and Ru^{II}−AQ compounds.

However, although the *p*-xylene spacer leads to significantly less π-conjugated systems than unsubstituted *p*-phenylene bridges,[33,34] some of the extinction in the 310−380 nm spectral range is likely to be caused by the molecular bridge and/or an increase of π-conjugation in the overall system. The TAA unit absorbs predominantly at shorter wavelengths and contributes substantially to the extinction below 300 nm.[35,36]

Expectedly, the osmium complexes from panel (b) exhibit the same spectral features as the isoelectronic ruthenium compounds, only that the ^{1}MLCT bands are red-shifted and that the ^{3}MLCT absorptions between 520 and 700 nm now become easily detectable as a consequence of the relaxation of spin selection rule. As in the case of ruthenium, the AQ unit causes the TAA−Os^{II}−AQ and Os^{II}−AQ molecules to absorb more strongly between 310 and 380 nm than the TAA−Os^{II} and Os^{II} molecules.

dx.doi.org/10.1021/ic300558s | Inorg. Chem. 2012, 51, 6333−6344

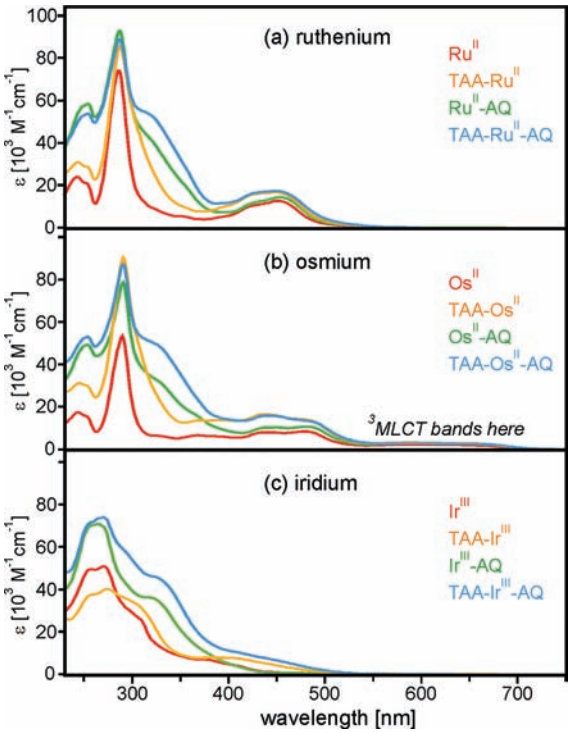

Figure 1. Optical absorption spectra of the 12 molecules from Scheme 2 in CH_3CN at 25 °C.

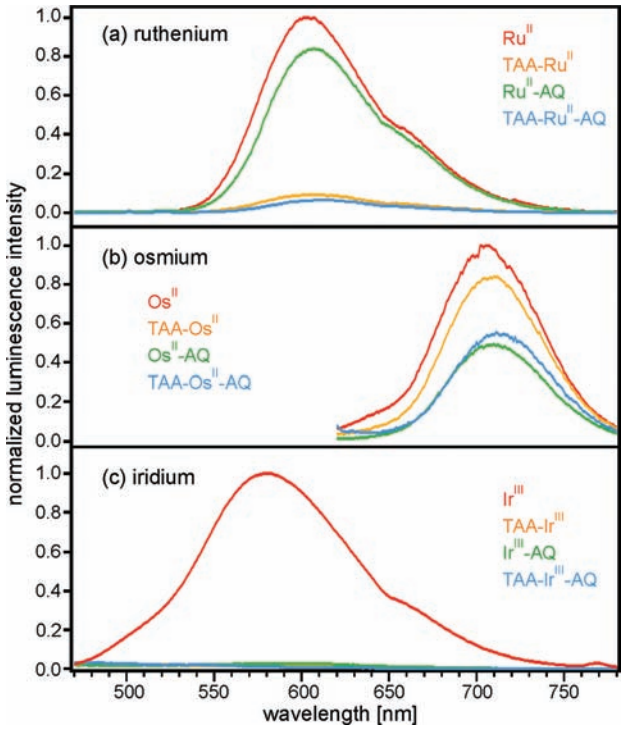

Figure 2. Luminescence spectra of the 12 molecules from Scheme 2 in aerated CH_3CN at 25 °C. Excitation occurred at 450 nm in the case of the ruthenium and osmium molecules (a, b) and at 380 nm in the case of the iridium molecules (c). Relative emission intensities were corrected for differences in sample absorbance at the excitation wavelength, and the final intensities were normalized to a value of 1.0 for the reference complexes (Ru^{II}, Os^{II}, Ir^{III}).

The cyclometalated iridium complexes in panel (c) exhibit ^{1}MLCT and ^{3}MLCT absorptions in the 400−500 nm spectral range, and to the higher energy side these absorptions merge directly into intraligand $\pi-\pi^*$ absorptions. Thus, it is difficult to perform a clear distinction between absorptions that involve the metal center and absorptions which do not. Be that as it may, the global appearance of all absorption spectra in Figure 1 is that expected for d^6 metal complexes of this type.[11,37−42] The dyad and triad spectra of the ruthenium and osmium triads correspond more or less (but not precisely) to the sum of the absorption spectra of the individual molecular components, indicating that the overall systems are electronically weakly coupled. At donor−photosensitizer and photosensitizer−acceptor distances of roughly 4.3 Å (i. e., the length of one *p*-xylene spacer), this is to be expected. However, for the TAA−Ir dyad and the TAA−Ir−AQ triad, the absorption spectra in Figure 1c reveal more pronounced interaction between the individual molecular moieties: There is a broad absorption band around 450 nm, in a spectral region where none of the individual components absorbs. Similar observations have been made previously in a TAA−$Ir(tpy)_2^{3+}$ dyad.[43]

Steady-State Luminescence Spectroscopy. All of the compounds from Scheme 2 are emissive when irradiating ~10^{-5} M (aerated) acetonitrile solutions of them with blue or UV light, albeit with widely varying luminescence intensities. Figure 2a shows the emission spectra of the four ruthenium compounds as detected after excitation at 450 nm. The luminescence intensity of the Ru^{II} reference complex has been normalized artificially to a value of 1.0; all other luminescence intensities are scaled relative to this reference point.[44] The Ru^{II}−AQ dyad exhibits an emission intensity practically on par with that of the ruthenium reference complex, while the TAA−Ru^{II} and TAA−Ru^{II}−AQ molecules emit an order of magnitude weaker. Both the AQ and TAA units have energetically high lying triplet excited states (~2.7 eV for AQ, ~3.2 eV for TAA);[45,46] hence excited-state deactivation by triplet−triplet energy transfer from the $Ru(bpy)_3^{2+}$ ^{3}MLCT excited state at 2.12 eV to either one of these two moieties is thermodynamically unlikely.[47−50] Subsequent sections will demonstrate that electron transfer from the TAA unit to the ruthenium complex is in fact the predominant excited-state deactivation pathway in the TAA−Ru^{II} and TAA−Ru^{II}−AQ molecules.

Expectedly, the ^{3}MLCT emissions of the osmium compounds in Figure 2b (excited at 450 nm) are all significantly red-shifted with respect to the ruthenium complexes in Figure 2a. The emission intensities of the Os^{II} reference complex and the TAA−Os^{II} dyad are similar, while those of the Os^{II}−AQ dyad and the TAA−Os^{II}−AQ triad are nearly a factor of 2 less intense. Since the emissive ^{3}MLCT state of the $Os(bpy)_3^{2+}$ complex is at even lower energy (1.79 eV)[51] than that of $Ru(bpy)_3^{2+}$, triplet−triplet energy transfer is even less probable in this case. Indeed, the subsequent sections will demonstrate that electron transfer from photoexcited osmium to AQ is an important excited-state deactivation channel.

Figure 2c shows the luminescence spectra obtained from the iridium complexes after excitation at 380 nm. For cyclometalated iridium(III) complexes of this type, the emission is commonly of mixed ^{3}MLCT/intraligand $\pi-\pi^*$ character.[40,42] Given the comparatively high energy of the emissive triplet states, excited-state deactivation by triplet−triplet energy transfer is an energetically more viable option for the iridium dyads and triads than for the ruthenium and osmium compounds. Nevertheless, the subsequent paragraphs of this paper will show that the strong emission quenching observed in

dx.doi.org/10.1021/ic300558s | Inorg. Chem. 2012, 51, 6333−6344

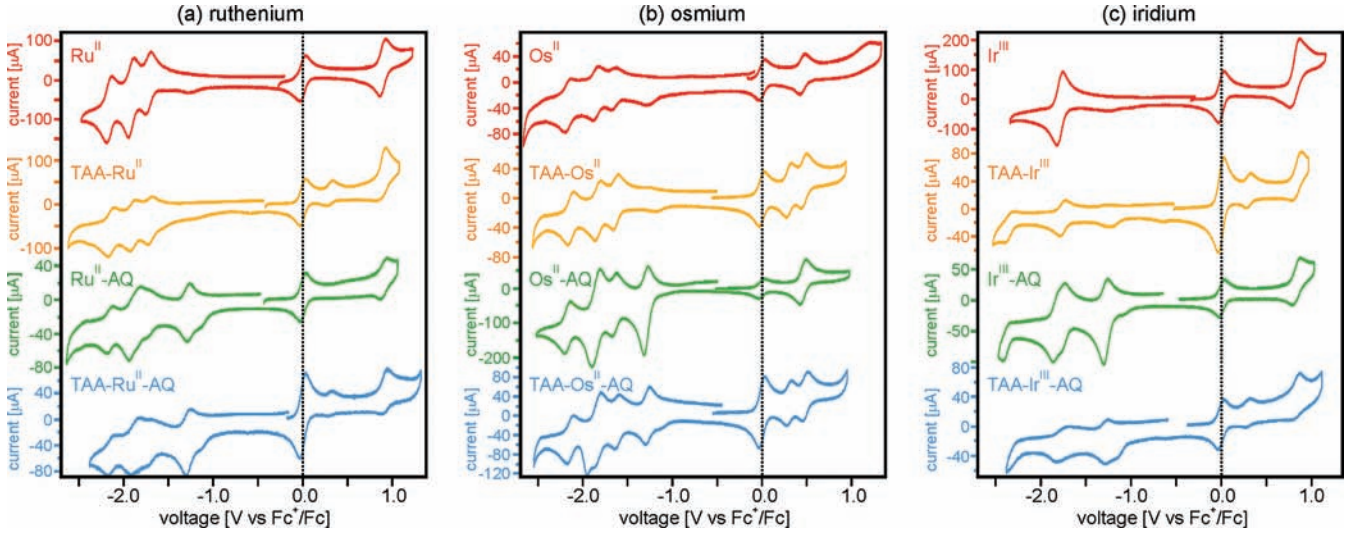

Figure 3. Cyclic voltammograms of the molecules from Scheme 2 in CH_3CN in the presence of 0.1 M $TBAPF_6$ as a supporting electrolyte. The waves at 0.0 V vs Fc^+/Fc (vertical dashed lines) are due to ferrocene, which was added in small quantities for internal voltage calibration.

the TAA–Ir^{III}, Ir^{III}–AQ, and TAA–Ir^{III}–AQ molecules is predominantly the consequence of efficient excited-state deactivation by photoinduced electron transfer.

To summarize this paragraph on the steady-state luminescence properties, we note that the *ruthenium* emission is quenched significantly in presence of the TAA donor while AQ has a weak influence, the *osmium* luminescence is quenched to a noticeable extent in the presence of AQ while TAA has a weak influence, and the *iridium* luminescence is strongly susceptible to the presence of both TAA and AQ.

Electrochemical Investigations and Energy Level Structure of the Triads. Figure 3 shows the cyclic voltammograms of the compounds in Scheme 2 as measured in acetonitrile solution in the presence of 0.1 M tetrabutylammonium hexafluorophosphate ($TBAPF_6$) as a supporting electrolyte. The reversible waves at 0.0 V vs Fc^+/Fc (dashed vertical lines) are due to ferrocene, which was added in small quantities to the solutions for internal voltage calibration. Vertical superposition of voltammograms from the reference complex (red traces), TAA–metal dyad (oranges traces), metal–AQ dyad (green traces), and TAA–metal–AQ triad (blue traces) in each of the three panels (a, b, c) permits unambiguous assignment of the individual redox waves. The reduction potentials extracted from the ruthenium compounds in Figure 3a are summarized in Table 1.

Oxidation of Ru(II) to Ru(III) occurs at a potential of 0.9 V vs Fc^+/Fc, in line with prior investigations.[38,39,52] Three bpy-localized reductions of the metal complex occur between −1.70 and −2.15 V vs Fc^+/Fc, also in agreement with literature values.[53,54] Although these are clearly ligand-centered reductions, for convenience we will later designate the first of these reduction processes as a reduction of the ruthenium(II) complex to a ruthenium(I) species (Ru^{II}/Ru^{I}). Oxidation of the TAA unit occurs at 0.30 V vs Fc^+/Fc, and reduction of AQ is at −1.27 V vs Fc^+/Fc, both in agreement with previously reported redox potentials for these moieties.[19,35,36,55−57] The fact that the redox potentials of all individual molecular components are nearly identical to those reported for their isolated counterparts is another indication that the molecular dyads and triads from Scheme 2 are electronically weakly coupled systems.

Table 1. Reduction Potentials for the Individual Redox-Active Components of the Ruthenium Molecules from Scheme 2[a]

	$Ru(bpy)_3^{2+}$	TAA–Ru^{II}	Ru^{II}–AQ	TAA–Ru^{II}–AQ
Ru(III/II)	0.89	0.89	0.90	0.92
$TAA^{+/0}$		0.30		0.30
$AQ^{0/-}$			−1.28	−1.27
$bpy^{0/-}$	−1.72	−1.70	−1.72	−1.73
$bpy^{0/-}$	−1.91	−1.90	−1.90	−1.86
$bpy^{0/-}$	−2.15	−2.13	−2.14	−2.13

[a]All values were extracted from the data in Figure 3a and are reported versus the ferrocenium/ferrocene (Fc^+/Fc) couple in acetonitrile solution. bpy- and AQ-localized one-electron reductions as well as TAA- and metal-localized one-electron oxidations are found to exhibit peak separations near the expected 59 mV, but the oxidation processes have higher peak currents in the oxidative than in the reductive sweep (ratios vary between 1:1 and ∼30:1).

The osmium data in Figure 3b lead us to similar conclusions. Not surprisingly, the TAA, AQ, and bpy redox potentials are hardly affected by the change in metal (Table 2); only the metal oxidation process is susceptible to the replacement of Ru(II) by Os(II). The conversion of Os(II) to Os(III) occurs at ∼0.5 V

Table 2. Reduction Potentials for the Individual Redox-Active Components of the Osmium Molecules from Scheme 2[a]

	$Os(bpy)_3^{2+}$	TAA–Os^{II}	Os^{II}–AQ	TAA–Os^{II}–AQ
Os(III/II)	0.45	0.47	0.46	0.48
$TAA^{+/0}$		0.30		0.30
$AQ^{0/-}$			−1.29	−1.28
$bpy^{0/-}$	−1.67	−1.63	−1.65	−1.62
$bpy^{0/-}$	−1.86	−1.84	−1.85	−1.83
$bpy^{0/-}$	−2.16	−2.13	−2.17	−2.14

[a]All values were extracted from the data in Figure 3b and are reported versus the ferrocenium/ferrocene (Fc^+/Fc) couple in acetonitrile solution. All one-electron redox waves exhibit peak separations near the expected 59 mV. All redox waves exhibit current peak ratios near 1:1 when comparing the current peaks of oxidative and reductive sweeps.

dx.doi.org/10.1021/ic300558s | *Inorg. Chem.* 2012, 51, 6333−6344

vs Fc^+/Fc, again in line with previous investigations.[51] As noted above for ruthenium, reduction of the $Os(bpy)_3^{2+}$ complex occurs predominantly at the bpy ligands, but for convenience we will later designate the one-electron reduced osmium complex as Os^I.

The cyclic voltammograms for the iridium complexes in Figure 3c are less rich on the reductive side than the ruthenium and osmium data because there is only one (instead of three) ligand-based reduction process in the potential window considered here. The wave at −1.8 V vs Fc^+/Fc is assigned to a bpy-localized reduction process (Table 3), whereas the 2-(*p*-tolyl)pyridine ligands are apparently reduced only at significantly more negative potentials. By analogy to what was noted above for ruthenium and osmium, below we will designate the reduced iridium complex as Ir^{II}. Oxidation of the metal complex occurs at ∼0.84 V vs Fc^+/Fc, producing a species that will be designated as Ir^{IV}. This potential is 80 mV lower for the iridium triad and dyads compared to that of the free Ir^{III} complex (second row of Table 3). For the ruthenium and osmium compounds, the difference between the metal oxidation potentials of the free complexes and those of the dyads and triads ranges from 0 to 30 mV (Tables 1 and 2). Thus, its seems that interaction of the iridium photosensitizing unit with the TAA and AQ moieties is somewhat stronger than in the case of the ruthenium and osmium dyads and triads. This finding is in line with those from optical absorption spectroscopy (see above). The electrochemical potentials of the organic redox-active moieties (TAA and AQ) are essentially the same in all of the dyads and triads (Tables 1−3).

Table 3. Reduction Potentials for the Individual Redox-Active Components of the Iridium Molecules from Scheme 2[a]

	Ir^{III}	TAA−Ir^{III}	Ir^{III}−AQ	TAA−Ir^{III}−AQ
Ir(IV/III)	0.92	0.84	0.84	0.84
$TAA^{+/0}$		0.30		0.30
$AQ^{0/-}$			−1.28	−1.26
$bpy^{0/-}$	−1.79	−1.76	−1.80	−1.75

[a]All values were extracted from the data in Figure 3c and are reported versus the ferrocenium/ferrocene (Fc^+/Fc) couple in acetonitrile solution. The bpy- and AQ-localized reductions exhibit good reversibility. TAA- and iridium-localized one-electron oxidation waves show peak separations close to the expected 59 mW, but the ratio between the current peaks in oxidative and reductive sweeps ranges from ∼1:1 to ∼40:1.

On the basis of the electrochemical data from Figure 3 and Tables 1−3, one can establish the energy level diagram for the triads shown in Scheme 3. In doing so, we have neglected any effects arising from distance-dependent donor−acceptor interactions and have simply calculated energies for the individual states from differences in reduction potentials.[58] This procedure obviously yields crude estimates at best, and even though we indicate energies to two digits of electron volts, we note that the error bars associated with these values are on the order of 0.1 eV. The energies of the emissive excited states of the individual metal complexes (2.12 eV, 1.79 eV, 2.37 eV) represent the commonly used literature values.[11,31,38,39,51] In Scheme 3, these excited states are designated as $*Ru^{II}$, $*Os^{II}$, and $*Ir^{III}$.

Common to all three triads is the presence of a charge-separated state near 1.6 eV containing oxidized triarylamine (TAA^+), the metal complex in its initial state (Ru^{II}, Os^{II}, or Ir^{III}), and reduced anthraquinone (AQ^-). The energy of this final charge-separated state is obviously independent of the metal. Importantly, this state is energetically below all of the initially excited metal-localized emissive states; consequently, the final charge-separated state is energetically accessible irrespective of whether the ruthenium, osmium, or iridium triad is considered.

In all three triads, there are two possibilities for the formation of the final charge-separated state: (i) reductive quenching of the initially excited $*Ru^{II}$, $*Os^{II}$, and $*Ir^{III}$ species by TAA, followed by electron transfer from the now reduced Ru^I, Os^I, or Ir^{II} complexes to AQ, or (ii) oxidative quenching of the initially excited $*Ru^{II}$, $*Os^{II}$, and $*Ir^{III}$ species by AQ, followed by electron transfer from TAA to the now oxidized Ru^{III}, Os^{III}, or Ir^{IV} complexes. As seen from Scheme 3a, in the ruthenium system, possibility i is likely to dominate because the TAA^+−Ru^I−AQ state at 2.03 eV can be formed in an exergonic step from the initially excited TAA−$*Ru^{II}$−AQ level (at 2.12 eV), while formation of the TAA−Ru^{III}−AQ^- state (at 2.19 eV) is thermodynamically uphill. These thermodynamic considerations are consistent with the observation of a very weak emission quenching in the Ru^{II}−AQ dyad with respect to the Ru^{II} reference complex (Figure 2a), and a significant luminescence quenching in the TAA−Ru^{II} dyad and TAA−Ru^{II}−AQ triad relative to Ru^{II}.

Scheme 3. Energy Level Scheme Showing the Relevant Photoexcited and Charge-Separated States Which Can Be Formed in the Three Triads from Scheme 2

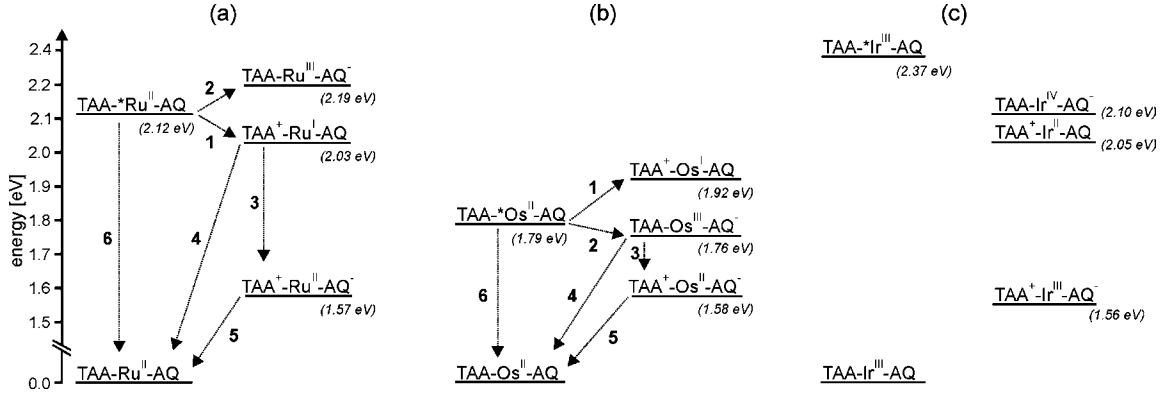

dx.doi.org/10.1021/ic300558s | Inorg. Chem. 2012, 51, 6333−6344

In the case of the osmium triad (Scheme 3b), the thermodynamic situation is different, and the oxidative quenching of the initially excited $*Os^{II}$ state is more probable: The $TAA^+-Os^{I}-AQ$ state is at 1.92 eV, which is roughly 0.13 eV above the initially excited ^{3}MLCT state. By contrast, the $TAA-Os^{III}-AQ^-$ level is at 1.76 eV, energetically close to the lowest ^{3}MLCT state of the $Os(bpy)_3^{2+}$ unit (at 1.79 eV); hence, the oxidative quenching appears thermodynamically more viable than the reductive quenching. Again, the luminescence data from Figure 2 is consistent with our energetic considerations: The emission intensity of the molecules containing AQ ($Os^{II}-AQ$ dyad and $TAA-Os^{II}-AQ$ triad) are weaker than those of the molecules that do not contain this oxidant (Os^{II}, $TAA-Os^{II}$ dyad), supporting the hypothesis that excited-state deactivation by electron transfer to anthraquinone is a more efficient process than reductive excited-state quenching by triarylamine in this case.

For the iridium triad, both the oxidative and reductive excited-state quenching processes are thermodynamically downhill from the initial $TAA-*Ir^{III}-AQ$ state at 2.37 eV: The $TAA-Ir^{IV}-AQ^-$ level is estimated to be at 2.10 eV; the $TAA^+-Ir^{II}-AQ$ state is calculated to lie at 2.05 eV. The observation of strong emission quenchings in both iridium dyads (including the triad) relative to the Ir^{III} reference complex is consistent with this energy level structure: irrespective of whether TAA or AQ is attached to the metal complex, nonradiative excited-state deactivation becomes efficient.

Nanosecond Transient Absorption. Figure 4 provides direct experimental evidence for the formation of the final charge-separated states containing oxidized TAA and reduced AQ. The series of transient absorption spectra shown in Figure 4a–c was measured using $\sim 10^{-5}$ M solutions of the $TAA-Ru^{II}-AQ$ (a), $TAA-Os^{II}-AQ$ (b), and $TAA-Ir^{III}-AQ$ (c) triads in deoxygenated acetonitrile.

In the case of the ruthenium and osmium systems, excitation occurred at 532 nm, while the iridium compound was excited at 355 nm. In all cases, the laser pulses had a width of ~10 ns. Detection took place in a time window of 200 ns starting immediately after the laser pulses. Under these experimental conditions, one obtains similar transient absorption spectra for all three triads. In each of the three spectra (Figure 4a–c), there are three bands with maxima near 380 nm, 565 nm, and 770 nm. On the basis of the spectro-electrochemical data in Figure 4d and e, the three bands can be readily assigned. Figure 4d shows a series of absorption spectra which were obtained while applying an electrochemical potential more positive than 0.5 V vs Fc^+/Fc to a CH_2Cl_2 solution of a triarylamine reference molecule (chemical structure shown in the inset). From this series of spectra (obtained after different time intervals after initiating the oxidation process; using 0.1 M $TBAPF_6$ as an electrolyte), we learn that the transient absorption band located around 770 nm is due to the oxidized amine.[35,36,55,59,60] The absorption spectra in Figure 4e were measured while applying an electrochemical potential more negative than −1.2 V vs Fc^+/Fc to a CH_2Cl_2 solution of 9,10-anthraquinone in the presence of 0.1 M $TBAPF_6$. From this series of spectra, we learn that the transient absorption bands located at 380 and 565 nm are due to reduced anthraquinone.[19,56,61,62] Thus, the observation of a fully charge-separated state in all three triads is beyond question, and this finding is in line with the energy level diagram from Scheme 3, in which we have come to the conclusion that such a final charge-separated state is thermodynamically accessible from the initially excited metal-localized state in all three triads.

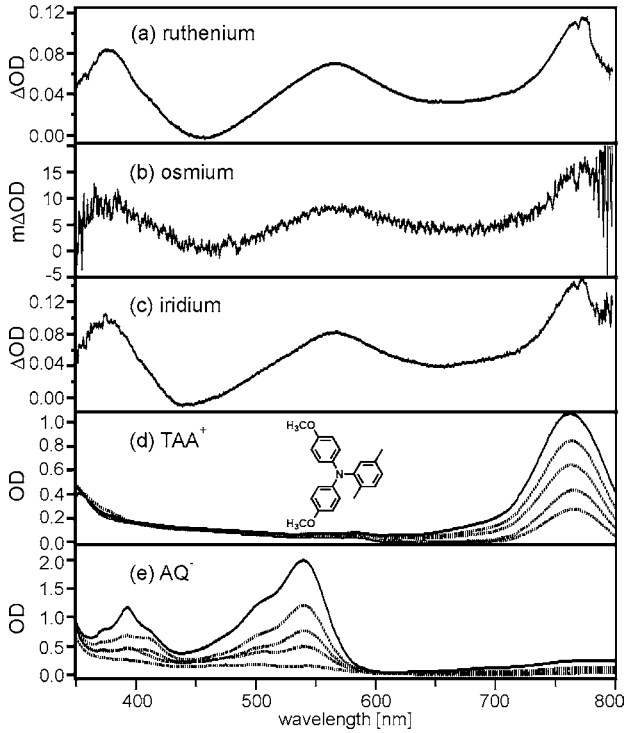

Figure 4. Panels a–c show transient absorption spectra measured on CH_3CN solutions of $TAA-Ru^{II}-AQ$ (a), $TAA-Os^{II}-AQ$ (b), and $TAA-Ir^{III}-AQ$ (c) in a 200-ns time window starting immediately after excitation with ~10-ns laser pulses at 532 nm (a, b) or 355 nm (c). Panel d shows a series of absorption spectra from a CH_2Cl_2 solution of a triarylamine reference molecule (structure shown in the inset) measured after increasing time intervals following the application of an electrochemical potential more positive than 0.5 V vs Fc^+/Fc (in presence of 0.1 M $TBAPF_6$). Panel e shows a series of absorption spectra obtained from a CH_2Cl_2 solution of 9,10-anthraquinone obtained in an analogous spectro-electrochemical experiment using potentials more negative than −1.2 V vs Fc^+/Fc.

Figure 5 shows the decays of the transient absorption intensities at 380 nm (black traces), 565 nm (blue traces), and 770 nm (green traces) in deoxygenated acetonitrile solution. In all three triads, we observe decays which are single exponential over at least 1 order of magnitude, and in all cases the decays at the three above-mentioned wavelengths yield nearly identical lifetimes. This is consistent with the notion that the TAA^+ and AQ^- species disappear jointly in a thermal charge-recombination event. The average lifetimes of the fully charge-separated states extracted from fits to the experimental decay data in Figure 5 are 1.3 μs in the case of the $TAA^+-Ru^{II}-AQ^-$ state,[29] 80 ns for the $TAA^+-Os^{II}-AQ^-$ state, and 890 ns in the case of the $TAA^+-Ir^{III}-AQ^-$ state (all in deoxygenated CH_3CN at 25 °C).[63]

Given the fact that the final charge-separated state involves electron–hole separation formally over a 22-Å distance, a lifetime in the 100-ns-to-μs regime is not particularly surprising,[1] even if the effective electron transfer distance may be somewhat shorter as a consequence of partial hole or electron delocalization onto the *p*-xylene bridging elements.[64–66] What *is* surprising, however, is the observation of a markedly shorter lifetime for the osmium triad compared to the ruthenium and iridium systems. We can only speculate what

dx.doi.org/10.1021/ic300558s | Inorg. Chem. 2012, 51, 6333–6344

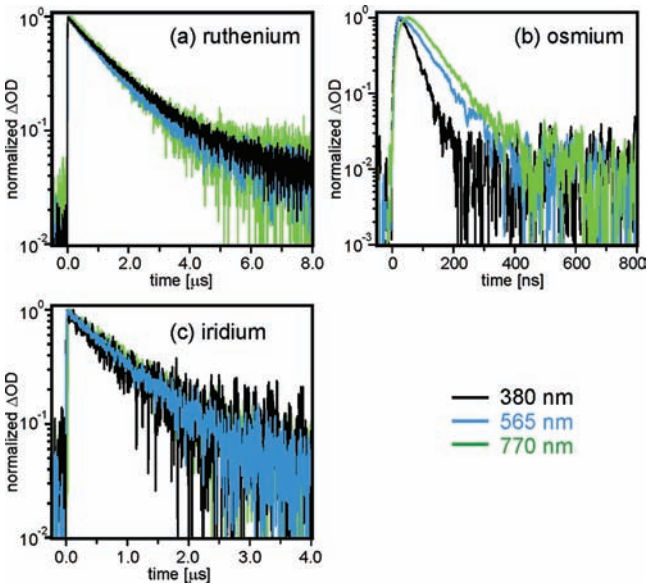

Figure 5. Decays of the transient absorption intensities from Figure 4 at three different wavelengths in the TAA–Ru^{II}–AQ (a), TAA–Os^{II}–AQ (b), and TAA–Ir^{III}–AQ (c) triads in deoxygenated CH_3CN solution at 25 °C. Excitation occurred at 532 nm for the ruthenium and osmium triads and at 355 nm for the iridium system.

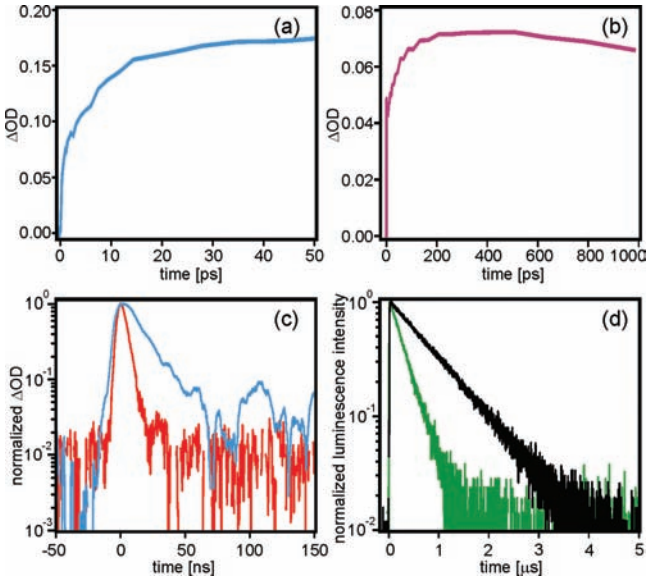

Figure 6. (a) Temporal evolution of the transient absorption signal at 770 nm (TAA^+ formation) after excitation of the TAA–Ru^{II}–AQ triad at 400 nm with laser pulses of 150 fs width. (b) Time profile for the transient absorption signal at 550 nm (AQ^- formation) in the same experiment. (c) Blue trace: Decay of the TAA^+ absorption at 770 nm in the TAA–Ru^{II} dyad after excitation at 450 nm with ~10-ns laser pulses. Red trace: Instrument response curve. (d) Black trace: Decay of the luminescence emitted by Ru^{II} at 610 nm in deoxygenated CH_3CN after excitation at 450 nm. Green trace: decay of the same luminescence in Ru^{II}–AQ in deoxygenated CH_3CN.

the origin of this effect might be, but it seems possible that the energetic proximity of the TAA–Os^{III}–AQ^- state, only 0.18 eV above the final charge-separated state, may play a role. In the ruthenium and iridium triads, the final charge-separated states are energetically well below all of the other states (>0.45 eV); hence, thermal one-step back-electron transfers might be less likely to occur in these systems than in the osmium triad. Be that as it may, we conclude from this section that the final charge-separated states containing TAA^+ cations and AQ^- anions are formed in all three triads from Scheme 2. In the following, we focus on the kinetics and quantum yields of their formation.

Kinetics and Quantum Yields for Formation of Charge-Separated States in the Ruthenium Triad. Figure 6a shows the build-up of the transient absorption intensity at 770 nm after photoexcitation of the TAA–Ru^{II}–AQ triad in acetonitrile at 400 nm. The pulse width in this case was 150 fs; hence, we are able to monitor the formation of TAA^+ at high temporal resolution in this experiment. The rise time for this transient absorption is 9 ps, and we may conclude that the TAA^+–Ru^{I}–AQ state at 2.03 eV is formed with a time constant of 1.1×10^{11} s^{-1} from the initially excited TAA–*Ru^{II}–AQ state at 2.12 eV. In Scheme 3 and Table 4, this particular electron transfer event, corresponding to a reductive $Ru(bpy)_3^{2+}$ ^{3}MLCT excited-state quenching by TAA, is denoted as process "1".

Figure 6b shows the temporal evolution of the transient absorption intensity for the same sample as in Figure 6a and in the same experiment, but detected at 550 nm. The rise time in this case is 50 ps, and we conclude that AQ^- is formed with a time constant of 2×10^{10} s^{-1}. Given the rapid kinetics for the formation of the TAA^+–Ru^{I}–AQ state at 2.03 eV, a time constant of 2×10^{10} s^{-1} is attributed to process "3" in Scheme 3, i.e., the electron transfer from Ru^I to AQ while maintaining the hole at the TAA^+ site. Already after ~200 ps the transient absorption intensities at 770 and 550 nm have both reached their maxima, indicating that the final charge-separated state

Table 4. Rate Constants for the Individual Intramolecular Processes Shown in Schemes 3 and 4 As Extracted from the Data in Figures 5–8 (Deoxygenated CH_3CN Solution, 25°C)

reaction step no.[a]	TAA–Ru^{II}–AQ	TAA–Os^{II}–AQ	TAA–Ir^{III}–AQ
1	1.1×10^{11} s^{-1}	$<5.3 \times 10^6$ s^{-1}	3.5×10^{12} s^{-1}
2	2.1×10^6 s^{-1}	$\sim 10^8$ s^{-1}	3.3×10^{11} s^{-1}
3	2.0×10^{10} s^{-1}	$\sim 10^8$ s^{-1}	2.5×10^{10} s^{-1}
4	6.7×10^7 s^{-1}	3.8×10^7 s^{-1}	1.5×10^7 s^{-1}
5	7.7×10^5 s^{-1}	1.3×10^7 s^{-1}	1.1×10^6 s^{-1}
6	1.2×10^6 s^{-1}	5.3×10^7 s^{-1}	4.4×10^6 s^{-1}

[a]Refers to the reaction steps marked by the numbered arrows in Schemes 3 and 4.

(TAA^+–Ru^{II}–AQ^-) at 1.57 eV is completely formed at this point. As discussed in the prior section, this state has a lifetime of 1.3 μs in deoxygenated CH_3CN, corresponding to a rate constant of 7.7×10^5 s^{-1} for process "5" in Scheme 3a (Table 4).

In the TAA–Ru^{II} dyad, the TAA^+ radical cation absorption at 770 nm decays with a lifetime of 15 ns (blue trace in Figure 6c). We infer from this observation that, in the triad, process "4" (Scheme 3a) proceeds with a rate constant of 6.7×10^7 s^{-1}. Thus, once the TAA^+–Ru^{I}–AQ state at 2.03 eV is formed, the system is much more likely to undergo ruthenium-to-anthraquinone electron transfer ($k_3 = 2 \times 10^{10}$ s^{-1}) than ruthenium-to-triarylamine back-electron transfer ($k_4 = 6.7 \times 10^7$ s^{-1}).

In order to estimate the quantum yield for the formation of the TAA^+–Ru^{II}–AQ^- state at 1.57 eV out of the initially excited TAA–*Ru^{II}–AQ state, two pieces of information are yet missing: (i) the rate constant for the reductive excited-state

dx.doi.org/10.1021/ic300558s | Inorg. Chem. 2012, 51, 6333–6344

quenching to form the TAA−Ru^{III}−AQ^- state at 2.19 eV (process "2" in Scheme 3a) and (ii) the decay rate constant of the $Ru(bpy)_3^{2+}$ ^{3}MLCT excited state (process "6" in Scheme 3a). The rate constant for process "6" may simply be estimated from the lifetime of the isolated $Ru(bpy)_3^{2+}$ complex in deoxygenated acetonitrile (1.2×10^6 s^{-1}). The rate constant for process "2" is more difficult to obtain. We have found that the only viable possibility in this case involves the use of time-resolved luminescence spectroscopy: Figure 6d compares the luminescence decays of the Ru^{II} reference complex (black trace) and the Ru^{II}−AQ dyad (green trace), detected at 610 nm after the excitation at 532 nm with laser pulses of ∼10 ns width. The luminescence decays with a lifetime of 830 ns in the case of the reference complex, and with a lifetime of 300 ns in the case of the Ru^{II}−AQ dyad. The difference between the two luminescence decay rate constants (2.1×10^6 s^{-1}) is taken as the rate constant for process "2" in Scheme 3. Unfortunately, the AQ^- anion cannot be detected for the Ru^{II}−AQ dyad,[57] presumably because of rapid thermal back-electron transfer in the opposite sense; this appears to be not an uncommon problem for ruthenium−quinone dyads.[25,57,74] In the triad, AQ^- is formed after TAA^+ (50 ps vs 9 ps, see above); hence in the picosecond transient absorption data (Figure 6a, b), one observes the formation of the final charge-separated state at 1.57 eV rather than the TAA−Ru^{III}−AQ^- state at 2.19 eV.

With numerical estimates for the rate constants of the processes "1" through "6" from Scheme 3a at hand (second column of Table 4), we estimate a quantum yield of 99.7% for the formation of the final charge-separated state. Essentially every photon put into the $Ru(bpy)_3^{2+}$ ^{3}MLCT state at 2.12 eV thus leads to the formation of a molecule in the TAA^+−Ru^{II}−AQ^- state at 1.57 eV.

Kinetics and Quantum Yields for Formation of Charge-Separated States in the Osmium Triad. In the case of the osmium triad, a completely different situation is encountered. The reductive excited-state quenching by TAA is endergonic in this sample, and we have been unable to find any evidence for the formation of the TAA^+−Os^I−AQ state at 1.92 eV, from investigations of both the TAA−Os^{II} dyad and the TAA−Os^{II}−AQ triad, in the pico- to millisecond time regimes. We conclude from this observation that the rate constant for process "1" in Scheme 3b amounts to less than 10% of the inherent $Os(bpy)_3^{2+}$ ^{3}MLCT decay rate constant, which is 5.3×10^7 s^{-1} under these experimental conditions (deoxygenated CH_3CN at room temperature; process "6" in Scheme 3b).[51]

In transient absorption experiments performed with the Os^{II}−AQ dyad and the TAA−Os^{II}−AQ triad, the radical anion of AQ (monitored at 550 nm) is formed with a time constant of ∼10 ns (Figure 7a, green trace). There is a technical problem associated with this finding: on the one hand, 10 ns is too long to be measured accurately with our femtosecond equipment, and on the other hand, 10 ns is too short to be detected on our nanosecond setup with reliable accuracy. In this awkward situation we tentatively attribute a rate constant of ∼10^8 s^{-1} to process "2" from Scheme 3b but note that error bars are rather large in this particular case.

In the Os^{II}−AQ dyad, the AQ^- signal at 550 nm decays with a time constant of 26 ns (Figure 7b), and consequently we estimate a rate constant of 3.8×10^7 s^{-1} for process "4" in Scheme 3b, which corresponds to back-electron transfer from reduced anthraquinone to Os^{III}.

For the TAA−Os^{II}−AQ triad, the transient absorption intensity at 770 nm, due to TAA^+, builds up with a time

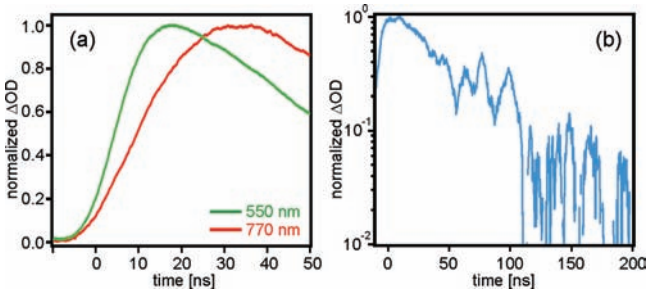

Figure 7. (a) Rise of the transient absorption signals at 550 nm (green trace) and 770 nm (red trace) after excitation of the TAA−Os^{II}−AQ triad at 532 nm with laser pulses of ∼10 ns width (CH_3CN solution). (b) Decay of the transient absorption signal of the Os^{II}−AQ dyad at 550 nm (AQ^- disappearance) after excitation at 532 nm with laser pulses of ∼10 ns width (deoxygenated CH_3CN solution).

constant of 20 ns (Figure 7a, red trace). Assuming process "2" has $k_2 \approx 10^8$ s^{-1} and further assuming that the TAA−Os^{III}−AQ^- state at 1.76 eV must be formed before the fully charge-separated state is accessible, we arrive at the conclusion that the rate constant for process "3" is ∼10^8 s^{-1}. The TAA^+−Os^{II}−AQ^- state at 1.58 eV then decays with a lifetime of 80 ns (see prior section), corresponding to a rate constant of 1.3×10^7 s^{-1} for process "5" in Scheme 3b. The complete set of rate constants for the TAA−Os^{II}−AQ triad in the third column of Table 4 leads us to the conclusion that the fully charge-separated state is formed with a quantum yield of ∼46% out of the initially excited $Os(bpy)_3^{2+}$ ^{3}MLCT state.

Kinetics and Quantum Yields for Formation of Charge-Separated States in the Iridium Triad. For the iridium triad, the situation is fundamentally different from that for the ruthenium and osmium triads: we were unable to selectively excite the metal complex in TAA−Ir^{III}−AQ. Even at the comparatively long wavelength of 420 nm there is an absorption from the organic moieties; this is particularly evident from a comparison of the (ground-state) absorption spectrum of the Ir^{III} reference complex with those of the TAA−Ir^{III} dyad and the TAA−Ir^{III}−AQ triad (Figure 1c). Instead of Scheme 3c, we therefore use an energy level diagram for the TAA−Ir^{III}−AQ triad which has been adapted to reflect this additional complication (Scheme 4). In this more complex scheme, we introduce an additional state named *(TAA−Ir^{III})−AQ, which is supposed to reflect the possibility that initial excitation may involve the entire triarylamine-iridium(III) fragment and not just solely the Ir^{III} complex. In addition to the evidence from absorption spectra, evidence for electronic interaction between the iridium complex and TAA was obtained from the electrochemical measurements, where a clear shift in the iridium oxidation potential was observed for the dyads and the triad (see above). Furthermore, in Scheme 4 we omit the TAA−Ir^{IV}−AQ^- state at 2.10 eV because there is no experimental evidence for its formation in the triad, see below.

The red trace in Figure 8a is the transient absorption spectrum detected with a delay of 1 ps after the excitation of TAA−Ir^{III}−AQ in CH_3CN at 420 nm. This spectrum shows an absorption band at 770 nm, which we have identified above as due to TAA^+. There is an additional absorption between 500 and 650 nm, which cannot be accounted for by the oxidized triarylamine unit (compare to Figure 4d). It appears plausible to attribute this additional absorption to the reduced metal complex, i.e., the Ir^{II} species. In the TAA−Ir^{III} dyad, a similar

dx.doi.org/10.1021/ic300558s | Inorg. Chem. 2012, 51, 6333−6344

Scheme 4. Energy Level Scheme Showing the Relevant Photoexcited and Charge-Separated States Which Can Be Formed in the Iridium Triad

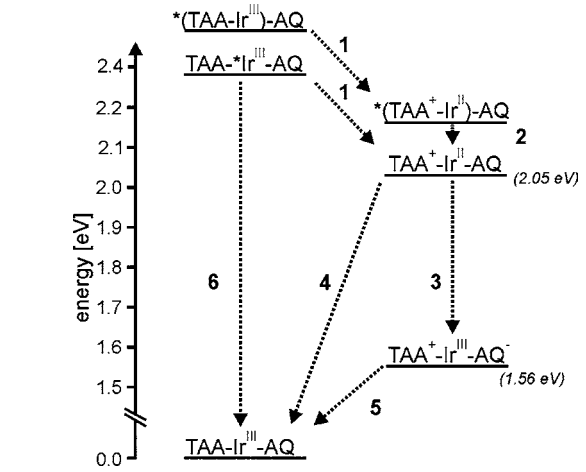

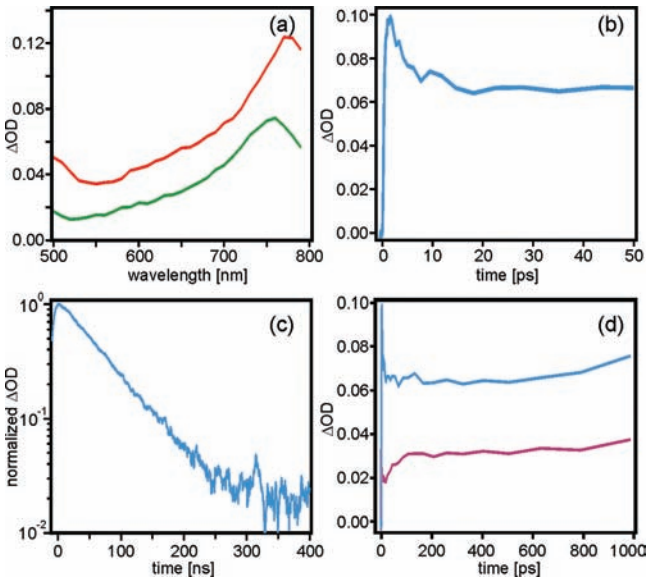

Figure 8. (a) Red trace: Transient absorption spectrum detected with a delay of 1 ps after excitation of an acetonitrile solution of TAA–Ir^{III}–AQ at 420 nm. Green trace: transient absorption spectrum from the same sample detected with a delay of 3 ps. (b) Time profile of the transient absorption at 770 nm from the same sample after excitation at 420 nm with laser pulses of 150 fs width. (c) Decay of the transient absorption at 770 nm after excitation of the TAA–Ir^{III} dyad (in deoxygenated CH_3CN) at 355 nm with ~10-ns laser pulses. (d) Time profiles of the transient absorption at 550 nm (purple trace) and 770 nm (blue trace) after 420-nm excitation of the TAA–Ir^{III}–AQ triad in CH_3CN (laser pulse width: 150 fs).

transient absorption spectrum can be detected in a 200-ns time window starting immediately after a 10-ns laser pulse (data not shown).

The time profile of the optical density at 770 nm after excitation of the iridium triad at 420 nm with femtosecond laser pulses is shown in Figure 8b. From the initial rise, we extract a time constant of 0.4 ps. Subsequently, there is a decrease in the ΔOD at this detection wavelength, occurring with a time constant of 3 ps. The spectral changes that occur in this time regime are minor (green trace in Figure 8a); hence, the electronic states formed after 0.4 ps (red trace in Figure 8a) and 3 ps (green trace in Figure 8a) must be chemically very similar to each other. In Scheme 4, we designate the state formed after 0.4 ps as *(TAA$^+$–Ir^{II})–AQ, while the state formed after 3 ps is denoted as TAA$^+$–Ir^{II}–AQ. In other words, after 0.4 ps a charge-separated state is already formed, but this state undergoes subsequent electronic relaxation with a time constant of 3 ps. In our opinion, this explanation makes sense in view of the fact that photoexcitation of the TAA–Ir^{III}–AQ triad (contrary to the ruthenium and osmium systems) cannot occur selectively at the metal center but seems to involve the entire TAA–Ir^{III} fragment, see above. Thus, in Scheme 4, we attribute a rate constant of 3.5×10^{12} s^{-1} to process "1" and a rate constant of 3.3×10^{11} s^{-1} to process "2" (last column of Table 4).

Once formed, the relaxed TAA$^+$–Ir^{II}–AQ state at 2.05 eV can either undergo charge-recombination to the ground state (process "4" in Scheme 4) or it can proceed to the final charge-separated state at 1.56 eV (process "3"). Experiments on the TAA–Ir^{III} dyad indicate that the back-electron transfer between the oxidized TAA and reduced iridium takes place with a time constant of 67 ns; the respective transient absorption decay data are shown in Figure 8c. We infer that in the triad, process "4" occurs with a rate constant of 1.5×10^7 s^{-1} (last column of Table 4).

Kinetic information regarding the formation of the fully charge-separated state at 1.56 eV can be extracted from the purple trace in Figure 8d, which shows the time profile of the optical density at 550 nm, i.e., at one of the absorption band maxima of the AQ^- species. The respective time profile shows an initial rapid rise and a decay due to the formation of the *(TAA$^+$–Ir^{II})–AQ and TAA$^+$–Ir^{II}–AQ states, which also absorb at this wavelength (Figure 8a). Subsequently, there is a slower rise with a time constant of 40 ps, which is attributed to the build-up of the TAA$^+$–Ir^{III}–AQ^- population. At the same time, the optical density at 770 nm stays essentially constant (blue trace in Figure 8d), consistent with the formation of the fully charge-separated state. A rate constant of 2.5×10^{10} s^{-1} is therefore attributed to process "3" in Scheme 4.

The rate constant for process "5", i.e., thermal charge-recombination from the TAA$^+$–Ir^{III}–AQ^- state at 1.56 eV, is 1.1×10^6 s^{-1} (lifetime of 890 ns, see prior section). The rate constant for process "6", i.e., relaxation of the photoexcited iridium complex to the electronic ground state, is estimated from the luminescence lifetime of the Ir^{III} reference complex (230 ns in oxygen-free acetonitrile; $k_6 = 4.4 \times 10^6$ s^{-1}).[31]

On the basis of the rate constants for the individual photophysical and photochemical processes in Scheme 4 (last column of Table 4), we arrive at the conclusion that the fully charge-separated state is formed in essentially quantitative yield from the initially photoexcited state.

■ SUMMARY AND CONCLUSIONS

Final charge-separated states containing an oxidized triarylamine fragment and a reduced anthraquinone moiety are formed in all three triads from Scheme 2, albeit with different quantum yields and via differing reaction mechanisms involving different kinetics. The thermodynamics of the photoinduced charge-separation steps are such that reductive quenching of the initially excited ruthenium state is clearly favored kinetically, while oxidative quenching is predominant in the case of the osmium system. In the iridium triad both the reductive and oxidative excited-state quenching steps are thermodynamically

dx.doi.org/10.1021/ic300558s | Inorg. Chem. 2012, 51, 6333–6344

possible, but the reductive pathway dominates kinetically. In the ruthenium and iridium systems, the driving forces associated with the formation of initial charge-separated states are sufficiently large to make photoinduced electron transfer the dominant excited-state deactivation pathway, particularly in view of the comparatively long ^{3}MLCT lifetimes of the $Ru(bpy)_3^{2+}$ and $[Ir(2\text{-}(p\text{-tolyl})pyridine)_2(bpy)]^+$ photosensitizers. From the initial charge-separated states, the formation of the final charge-separated state is kinetically favored versus thermal recombination in all three cases, which may be a manifestation of an inverted driving-force effect.[47,67] These favorable circumstances lead to the formation of the final charge-separated state with quantum yields near unity, at least in the case of the ruthenium and iridium systems. The osmium triad, by contrast, suffers from a much shorter ^{3}MLCT lifetime of the $Os(bpy)_3^{2+}$ sensitizer and a significantly lower driving force for formation of the initial charge-separated state, leading to a quantum yield around 0.46 for formation of the fully charge-separated state.

The lifetimes of the fully charge-separated states are in the microsecond regime in the ruthenium and iridium triads. Three factors may be responsible for these slow recombination kinetics: (i) an inverted driving-force effect,[47,67] (ii) a long electron−hole separation distance (~22 Å),[68,69] and (iii) spin selection rule.[70] In the case of the osmium triad, the lifetime of the fully charge-separated state is more than an order of magnitude shorter than in the ruthenium and iridium systems, possibly because of a relatively small energy gap between the $TAA-Os^{III}-AQ^-$ state and the $TAA^+-Os^{II}-AQ^-$ state. It thus appears that a large energy gap (here, > 0.45 eV) to the energetically next higher lying electronic state is another important ingredient for obtaining a long-lived final charge-separated state. We think this is an important new finding; one would have expected much more similar lifetimes for the charge-separated states of the three triads. The fact that we were able to compare a nearly isostructural series of linear donor−sensitizer−acceptor compounds is a significant advantage in this context.

Future work on these systems will focus on the role of coupling of intramolecular photoinduced electron transfer to bimolecular proton transfer with reduced anthraquinone as a proton-accepting site. Preliminary results from this work have been communicated recently.[71]

EXPERIMENTAL SECTION

The syntheses of the organic moieties of the rigid rod-like molecular triads and dyads (triarylamine-2,2′-bipyridine-anthraquinone unit for the triad; triarylamine-2,2′-bipyridine and 2,2′-bipyridine-anthraquinone units for the dyads) were described in detail in the Supporting Information to one of our previous publications.[29] Reaction of the individual functionalized bpy ligands with $Ru(bpy)_2Cl_2$, $Os(bpy)_2Cl_2$, and $[Ir(2\text{-}(p\text{-tolyl})pyridine)_2Cl]_2$ precursors occurred following standard protocols.[30−32] Briefly, a mixture of the starting materials in ethylene glycol was refluxed overnight under N_2. After cooling to room temperature, water was added, and the aqueous phase was extracted with CH_2Cl_2. The organic phase was dried over $MgSO_4$, and the solvent was removed under reduced pressure. Product purification occurred by column chromatography on silica gel using a mixture of acetone/water/aqueous saturated KNO_3 solution (90/9/1) as the eluent. The desired product was precipitated from the aqueous solution (after acetone removal) by the addition of saturated aqueous KPF_6 solution.

Product characterization data for $TAA-Ru^{II}-AQ$, $TAA-Ru^{II}$, and $Ru^{II}-AQ$ (including ligands for the dyads) have been reported previously.[29,57] For all other (new) molecules, they are as follows:

$TAA-Os^{II}$. Obtained in 68% yield (53 mg) from 30 mg of free ligand[29] and 35 mg of $Os(bpy)_2Cl_2$. ^{1}H NMR (300 MHz, CD_2Cl_2, 25 °C): δ [ppm] 1.79 (s, 3 H, CH_3), 1.90 (s, 3 H, CH_3), 3.73 (s, 6 H, OCH_3), 6.76 (m, 9 H), 6.95 (s, 1 H, xy), 7.36 (m, 5 H), 7.61 (m, 6 H), 7.86 (m, 6 H), 8.41 (m, 6 H). ES-MS: m/z 495.66 (calculated 495.66 for $C_{52}H_{45}N_7O_2Os^{2+}$). Anal. Calcd. for $C_{52}H_{45}N_7O_2OsP_2F_{12}$: C, 48.79; H, 3.54; N, 7.66. Found: C, 48.44; H, 3.47; N, 7.50. (The abbreviation "xy" in the NMR data stands for aromatic protons of the *p*-xylene units).

$Os^{II}-AQ$. Obtained in 49% yield (64 mg) from 50 mg of free ligand[29] and 61 mg of $Os(bpy)_2Cl_2$. ^{1}H NMR (300 MHz, CD_3CN, 25 °C): δ [ppm] 2.02 (s, 3 H, CH_3), 2.25 (s, 3 H, CH_3), 7.12 (s, 1 H, xy), 7.22 (s, 1 H, xy), 7.32 (m, 5 H), 7.56 (d, J = 1.5 Hz, 1 H), 7.67 (m, 4 H), 7.83 (m, 4 H), 7.90 (m, 6 H), 8.12 (d, J = 1.6 Hz, 1 H), 8.29 (m, 3 H), 8.50 (m, 6 H). ES-MS: m/z 485.133 (calculated 485.135 for $C_{52}H_{38}N_6O_2Os^{2+}$). Anal. Calcd. for $C_{52}H_{38}N_6O_2OsP_2F_{12}\cdot 1.5\ H_2O$: C, 48.56; H, 3.21; N, 6.53. Found C, 48.66; H, 3.13; N, 6.49.

$TAA-Os^{II}-AQ$. Obtained in 72% yield from 30 mg of free ligand[29] and 21 mg of $Os(bpy)_2Cl_2$. ^{1}H NMR (300 MHz, CD_2Cl_2, 25 °C): δ [ppm] 1.81 (s, 3 H, CH_3), 1.91 (s, 3 H, CH_3), 1.97 (s, 3 H, CH_3), 2.34 (s, 3 H, CH_3), 3.74 (s, 6 H, OCH_3), 6.77 (m, 8 H, amine), 6.99 (s, 1 H), 7.14 (s, 1 H), 7.16 (s, 1 H), 7.35 (m, 2 H), 7.46 (m, 3 H), 7.57 (m, 2 H), 7.67 (m, 2 H), 7.73 (m, 1 H), 7.82 (m, 6 H), 7.92 (m, 4H), 8.20 (m, 1 H), 8.30 (m, 3 H), 8.45 (m, 4 H), 8.59 (m, 2 H). ES-MS: m/z 650.71 (calculated 650.71 for $C_{74}H_{59}N_7O_4Os^{2+}$). Anal. Calcd. for $C_{74}H_{59}N_7O_4OsP_2F_{12}\cdot 2H_2O$: C, 54.64; H, 3.90; N, 6.03. Found: C, 54.41; H, 3.79; N, 6.04.

$TAA-Ir^{III}$. Obtained in 73% yield (28 mg) from refluxing 28 mg of organic ligand[29] with 30 mg of $[Ir(2\text{-}(p\text{-tolyl})pyridine)_2Cl]_2$[30] in a mixture of ethanol (10 mL) and chloroform (3 mL). After cooling to room temperature and the addition of a saturated aqueous solution of KPF_6, a yellow-orange solid formed. This solid was filtered, washed with water and diethylether, and dried under a vacuum. ^{1}H NMR (300 MHz, CD_2Cl_2, 25 °C): δ [ppm] 1.80 (s, 3 H, CH_3), 1.92 (s, 3 H, CH_3), 2.11 (m, 6 H, CH_3), 3.73 (s, 6 H, OCH_3), 6.08 (s, 1 H), 6.15 (s, 1 H), 6.78 (m, 9 H), 6.93 (m, 5 H), 7.43 (m, 1 H), 7.56 (m, 4 H), 7.74 (m, 2 H), 7.88 (m, 2 H), 8.05 (m, 4 H), 8.51 (m, 2 H). ES-MS: m/z 1016.35 (calculated 1016.35 for $C_{56}H_{49}N_5O_2Ir^+$). Anal. Calcd. for $C_{56}H_{49}N_5O_2IrPF_6\cdot H_2O$: C, 57.04; H, 4.36; N, 5.94. Found: C, 57.10; H, 4.22; N, 5.87.

$Ir^{III}-AQ$. Obtained in 80% yield (24 mg) from 27 mg of organic ligand[29] and 30 mg of $[Ir(2\text{-}(p\text{-tolyl})pyridine)_2Cl]_2$[30] following the procedure described above for $TAA-Ir^{III}$. ^{1}H NMR (300 MHz, CD_3CN, 25 °C): δ [ppm] 1.99 (s, 3 H, CH_3), 2.07 (s, 3 H, CH_3), 2.11 (s, 3 H, CH_3), 2.27 (s, 3 H, CH_3), 6.12 (s, 1 H), 6.17 (s, 1 H), 6.88 (m, 2 H), 7.01 (m, 2 H), 7.16 (s, 1 H), 7.23 (s, 1 H), 7.52 (m, 1 H), 7.63 (m, 1 H), 7.69 (m, 3 H), 7.83 (m, 3 H), 7.90 (m, 2 H), 8.00 (m, 4 H), 8.17 (m, 3 H), 8.29 (m, 3 H), 8.57 (m, 2 H). ES-MS: m/z 995.29 (calculated 995.29 for $C_{56}H_{42}N_4O_2Ir^+$). Anal. Calcd. for $C_{56}H_{42}N_4O_2IrPF_6\cdot 0.3CHCl_3$: C, 57.50; H, 3.63; N, 4.76. Found: C, 57.74; H, 3.41; N, 4.73.

$TAA-Ir^{III}-AQ$. Obtained in 87% yield (34 mg) from 46 mg of organic ligand[29] and 30 mg of $[Ir(2\text{-}(p\text{-tolyl})pyridine)_2Cl]_2$[30] following the procedure described above for $TAA-Ir^{III}$. ^{1}H NMR (300 MHz, CD_2Cl_2, 25 °C): δ [ppm] 1.81 (s, 3 H, CH_3), 1.93 (s, 3 H, CH_3), 1.97 (s, 3 H, CH_3), 2.10 (m, 6 H, CH_3), 2.28 (s, 3 H, CH_3), 3.75 (s, 6 H, OCH_3), 6.15 (m, 2 H), 6.78 (m, 8 H, C_6H_4), 6.88 (m, 2 H), 6.99 (m, 3 H), 7.17 (m, 2 H), 7.62 (m, 4 H), 7.77 (m, 3 H), 7.83 (m, 2 H), 7.89 (m, 2 H), 8.10 (m, 2 H), 8.16 (m, 2 H), 8.30 (m, 5 H), 8.58 (m, 2 H). ES-MS: m/z 1326.45 (calculated 1326.45 for $C_{78}H_{63}N_5O_4IrPF_6$: C, 63.66; H, 4.32; N, 4.76. Found: C, 64.00; H, 4.45; N, 4.78.

^{1}H NMR spectroscopy was performed using Bruker Avance DRX 300 and Bruker B-ACS-120 spectrometers. A Finnigan MAT8200 instrument was employed for mass spectrometry, and elemental analysis was performed on a Vario EL III CHNS analyzer from Elementar. Cyclic voltammograms were obtained using a Versastat3−200 potentiostat from Princeton Applied Research. A glassy carbon disk was used as a working electrode. A silver wire served as a quasi-reference electrode, and a second silver wire was used as a

dx.doi.org/10.1021/ic300558s | Inorg. Chem. 2012, 51, 6333−6344

counterelectrode. Voltage sweeps occurred at rates of 100 mV/s; solutions were deoxygenated by bubbling N_2 gas prior to measurements. Optical absorption spectra were recorded on a Cary 300 spectrometer from Varian. Spectro-electrochemical experiments were performed using the Cary 300 spectrometer, the potentiostat mentioned above, and an optically transparent thin-layer (OTTLE) cell from Specac.[72] Steady-state luminescence spectra were measured on a Fluorolog-3 instrument (FL322) from Horiba Jobin-Yvon, equipped with a TBC-07C detector from Hamamatsu. Transient absorption and time-resolved luminescence in the nanosecond time domain was measured using an LP920-KS instrument from Edinburgh Instruments. The detection system of the LP920-KS spectrometer consisted of an R928 photomultiplier and an iCCD camera from Andor. The excitation source was a Quantel Brilliant b laser (frequency-doubled or -tripled). Prior to nanosecond time-resolved measurements, samples were thoroughly deoxygenated by bubbling N_2 gas through the solutions, or by using home-built quartz cuvettes and a freeze−pump−thaw technique for oxygen removal. The sample absorbance at the excitation wavelength was typically between 0.1 and 0.3. A pump−probe method for time-resolved absorption was used to detect fast processes with a time resolution of 150 fs. The femtosecond pulse generator (TISSA50, Avesta/CDP) was pumped with a continuous wave Nd:YAG second harmonic laser (Verdi-V6, Coherent). The femtosecond pulses were amplified with a Ti-Sapphire amplifier (Avesta/CDP) pumped by a Nd:YAG laser (LF114, Solar TII). After the amplifier, the beam was split in two separate beams. The first part was passed through a second harmonic generator to obtain excitation (pump) pulses at 400 or 420 nm, and the second part was passed through a cuvette with water to generate a white light continuum as the monitoring (probe) pulse. The excitation beam was directed to a delay line (Avesta/CDP), enabling measurements of the transient absorption spectra up to 1 ns after excitation. A monochromator (Andor 0032) and a CCD camera (Newton DU920N-BR-DD, Andor) were used to record the spectra. The sample was placed in a rotating cuvette to prevent any degradation due to the laser excitation. The obtained time-resolved absorption decay curves were globally fitted to a sum of exponentials. The instrumental setup and the data analysis procedure are described in more detail elsewhere.[73]

AUTHOR INFORMATION

Corresponding Author

*E-mail: helge.lemmetyinen@tut.fi (H.L.), oliver.wenger@chemie.uni-goettingen.de (O.S.W.).

Notes

The authors declare no competing financial interest.

ACKNOWLEDGMENTS

This work was supported by the Swiss National Science Foundation (SNSF) through Grant 200021-117578, by the Deutsche Forschungsgemeinschaft (DFG) through Grant INST186/872-1, and by the Academy of Finland.

REFERENCES

(1) Balzani, V. *Electron Transfer in Chemistry*; VCH Wiley: Weinheim, Germany, 2001; Vol. 3.
(2) Collin, J.-P.; Guillerez, S.; Sauvage, J.-P.; Barigelletti, F.; De Cola, L.; Flamigni, L.; Balzani, V. *Inorg. Chem.* **1991**, *30*, 4230−4238.
(3) Collin, J.-P.; Guillerez, S.; Sauvage, J.-P.; Barigelletti, F.; Flamigni, L.; De Cola, L.; Balzani, V. *Coord. Chem. Rev.* **1991**, *111*, 291−296.
(4) Collin, J.-P.; Guillerez, S.; Sauvage, J.-P.; Barigelletti, F.; De Cola, L.; Flamigni, L.; Balzani, V. *Inorg. Chem.* **1992**, *31*, 4112−4117.
(5) Sauvage, J.-P.; Collin, J.-P.; Chambron, J.-C.; Guillerez, S.; Coudret, C.; Balzani, V.; Barigelletti, F.; De Cola, L.; Flamigni, L. *Chem. Rev.* **1994**, *94*, 993−1019.
(6) Collin, J.-P.; Dixon, I. M.; Sauvage, J.-P.; Williams, J. A. G.; Barigelletti, F.; Flamigni, L. *J. Am. Chem. Soc.* **1999**, *121*, 5009−5016.
(7) Dixon, I. M.; Collin, J.-P.; Sauvage, J.-P.; Barigelletti, F.; Flamigni, L. *Angew. Chem., Int. Ed.* **2000**, *39*, 1292−1295.
(8) Dixon, I. M.; Collin, J.-P.; Sauvage, J.-P.; Flamigni, L.; Encinas, S.; Barigelletti, F. *Chem. Soc. Rev.* **2000**, *29*, 385−391.
(9) Chakraborty, S.; Wadas, T. J.; Hester, H.; Schmehl, R.; Eisenberg, R. *Inorg. Chem.* **2005**, *44*, 6865−6878.
(10) Goransson, E.; Boixel, J.; Monnereau, C.; Blart, E.; Pellegrin, Y.; Becker, H. C.; Hammarström, L.; Odobel, F. *Inorg. Chem.* **2010**, *49*, 9823−9832.
(11) Roundhill, D. M. *Photochemistry and Photophysics of Metal Complexes*; Plenum Press: New York, 1994.
(12) Baranoff, E.; Collin, J.-P.; Flamigni, L.; Sauvage, J.-P. *Chem. Soc. Rev.* **2004**, *33*, 147−155.
(13) Flamigni, L.; Collin, J.-P.; Sauvage, J.-P. *Acc. Chem. Res.* **2008**, *41*, 857−871.
(14) Abrahamsson, M.; Jager, M.; Osterman, T.; Eriksson, L.; Persson, P.; Becker, H. C.; Johansson, O.; Hammarström, L. *J. Am. Chem. Soc.* **2006**, *128*, 12616−12617.
(15) Abrahamsson, M.; Jager, M.; Kumar, R. J.; Osterman, T.; Persson, P.; Becker, H. C.; Johansson, O.; Hammarström, L. *J. Am. Chem. Soc.* **2008**, *130*, 15533−15542.
(16) Hammarström, L.; Johansson, O. *Coord. Chem. Rev.* **2010**, *254*, 2546−2559.
(17) Kumar, R. J.; Karlsson, S.; Streich, D.; Jensen, A. R.; Jager, M.; Becker, H. C.; Bergquist, J.; Johansson, O.; Hammarström, L. *Chem.—Eur. J.* **2010**, *16*, 2830−2842.
(18) Cooley, L. F.; Larson, S. L.; Elliott, C. M.; Kelley, D. F. *J. Phys. Chem.* **1991**, *95*, 10694−10700.
(19) Opperman, K. A.; Mecklenburg, S. L.; Meyer, T. J. *Inorg. Chem.* **1994**, *33*, 5295−5301.
(20) Larson, S. L.; Elliott, C. M.; Kelley, D. F. *J. Phys. Chem.* **1995**, *99*, 6530−6539.
(21) Treadway, J. A.; Chen, P. Y.; Rutherford, T. J.; Keene, F. R.; Meyer, T. J. *J. Phys. Chem. A* **1997**, *101*, 6824−6826.
(22) Rutherford, T. J.; Keene, F. R. *Inorg. Chem.* **1997**, *36*, 2872−2878.
(23) Klumpp, T.; Linsenmann, M.; Larson, S. L.; Limoges, B. R.; Bürssner, D.; Krissinel, E. B.; Elliott, C. M.; Steiner, U. E. *J. Am. Chem. Soc.* **1999**, *121*, 1076−1087.
(24) Maxwell, K. A.; Sykora, M.; DeSimone, J. M.; Meyer, T. J. *Inorg. Chem.* **2000**, *39*, 71−75.
(25) Borgström, M.; Johansson, O.; Lomoth, R.; Baudin, H. B.; Wallin, S.; Sun, L. C.; Åkermark, B.; Hammarström, L. *Inorg. Chem.* **2003**, *42*, 5173−5184.
(26) Falkenström, M.; Johansson, O.; Hammarström, L. *Inorg. Chim. Acta* **2007**, *360*, 741−750.
(27) Wenger, O. S. *Coord. Chem. Rev.* **2009**, *253*, 1439−1457.
(28) Dupont, N.; Ran, Y. F.; Jia, H. P.; Grilj, J.; Ding, J.; Liu, S. X.; Decurtins, S.; Hauser, A. *Inorg. Chem.* **2011**, *50*, 3295−3303.
(29) Hankache, J.; Wenger, O. S. *Chem. Commun.* **2011**, *47*, 10145−10147.
(30) Freys, J. C.; Bernardinelli, G.; Wenger, O. S. *Chem. Commun.* **2008**, 4267−4269.
(31) Hanss, D.; Freys, J. C.; Bernardinelli, G.; Wenger, O. S. *Eur. J. Inorg. Chem.* **2009**, 4850−4859.
(32) Sullivan, B. P.; Salmon, D. J.; Meyer, T. J. *Inorg. Chem.* **1978**, *17*, 3334−3341.
(33) Hanss, D.; Wenger, O. S. *Inorg. Chem.* **2008**, *47*, 9081−9084.
(34) Hanss, D.; Wenger, O. S. *Eur. J. Inorg. Chem.* **2009**, 3778−3790.
(35) Geiss, B.; Lambert, C. *Chem. Commun.* **2009**, 1670−1672.
(36) Sreenath, K.; Suneesh, C. V.; Gopidas, K. R.; Flowers, R. A. *J. Phys. Chem. A* **2009**, *113*, 6477−6483.
(37) Meyer, T. J. *Pure Appl. Chem.* **1986**, *58*, 1193−1206.
(38) Balzani, V.; Juris, A.; Venturi, M.; Campagna, S.; Serroni, S. *Chem. Rev.* **1996**, *96*, 759−833.
(39) Juris, A.; Balzani, V.; Barigelletti, F.; Campagna, S.; Belser, P.; Von Zelewsky, A. *Coord. Chem. Rev.* **1988**, *84*, 85−277.

(40) Lamansky, S.; Djurovich, P.; Murphy, D.; Abdel-Razzaq, F.; Kwong, R.; Tsyba, I.; Bortz, M.; Mui, B.; Bau, R.; Thompson, M. E. *Inorg. Chem.* **2001**, *40*, 1704−1711.
(41) McCusker, J. K. *Acc. Chem. Res.* **2003**, *36*, 876−887.
(42) Lowry, M. S.; Bernhard, S. *Chem.—Eur. J.* **2006**, *12*, 7970−7977.
(43) Baranoff, E.; Dixon, I. M.; Collin, J.-P.; Sauvage, J.-P.; Ventura, B.; Flamigni, L. *Inorg. Chem.* **2004**, *43*, 3057−3066.
(44) The absorbance at the excitation wavelength was typically in the range between 0.1 and 0.3. The individual luminescence intensities were corrected for differences in absorbance at the excitation wavelength.
(45) Turro, N. J. *Molecular Photochemistry*; W.A. Benjamin: New York, 1967.
(46) Marsal, P.; Avilov, I.; da Silva, D. A.; Bredas, J. L.; Beljonne, D. *Chem. Phys. Lett.* **2004**, *392*, 521−528.
(47) Schanze, K. S.; MacQueen, D. B.; Perkins, T. A.; Cabana, L. A. *Coord. Chem. Rev.* **1993**, *122*, 63−89.
(48) Schoonover, J. R.; Dattelbaum, D. M.; Malko, A.; Klimov, V. I.; Meyer, T. J.; Styers-Barnett, D. J.; Gannon, E. Z.; Granger, J. C.; Aldridge, W. S.; Papanikolas, J. M. *J. Phys. Chem. A* **2005**, *109*, 2472−2475.
(49) Simon, J. A.; Curry, S. L.; Schmehl, R. H.; Schatz, T. R.; Piotrowiak, P.; Jin, X. Q.; Thummel, R. P. *J. Am. Chem. Soc.* **1997**, *119*, 11012−11022.
(50) Freys, J. C.; Wenger, O. S. *Eur. J. Inorg. Chem.* **2010**, 5509−5516.
(51) Creutz, C.; Chou, M.; Netzel, T. L.; Okumura, M.; Sutin, N. *J. Am. Chem. Soc.* **1980**, *102*, 1309−1319.
(52) Walther, M. E.; Wenger, O. S. *Inorg. Chem.* **2011**, *50*, 10901−10907.
(53) Furue, M.; Maruyama, K.; Oguni, T.; Naiki, M.; Kamachi, M. *Inorg. Chem.* **1992**, *31*, 3792−3795.
(54) Anderson, P. A.; Keene, F. R.; Meyer, T. J.; Moss, J. A.; Strouse, G. F.; Treadway, J. A. *J. Chem. Soc., Dalton Trans.* **2002**, 3820−3831.
(55) Sreenath, K.; Thomas, T. G.; Gopidas, K. R. *Org. Lett.* **2011**, *13*, 1134−1137.
(56) Babaei, A.; Connor, P. A.; McQuillan, A. J.; Umapathy, S. *J. Chem. Educ.* **1997**, *74*, 1200−1204.
(57) Hankache, J.; Wenger, O. S. *Phys. Chem. Chem. Phys.* **2012**, *14*, 2685−2692.
(58) Weller, A. *Z. Phys. Chem.* **1982**, *133*, 93−98.
(59) Lambert, C.; Nöll, G. *J. Am. Chem. Soc.* **1999**, *121*, 8434−8442.
(60) Hankache, J.; Wenger, O. S. *Chem. Rev.* **2011**, *111*, 5138−5178.
(61) Lewis, F. D.; Thazhathveetil, A. K.; Zeidan, T. A.; Vura-Weis, J.; Wasielewski, M. R. *J. Am. Chem. Soc.* **2010**, *132*, 444−445.
(62) Mecklenburg, S. L.; McCafferty, D. G.; Schoonover, J. R.; Peek, B. M.; Erickson, B. W.; Meyer, T. J. *Inorg. Chem.* **1994**, *33*, 2974−2983.
(63) The shorter lifetime of the fully charge-separated state in the osmium triad explains the lower signal-to-noise ratio in the transient absorption spectrum of Figure 4b relative to those of Figure 4a/c.
(64) Lancaster, K.; Odom, S. A.; Jones, S. C.; Thayumanavan, S.; Marder, S. R.; Brédas, J. L.; Coropceanu, V.; Barlow, S. *J. Am. Chem. Soc.* **2009**, *131*, 1717−1723.
(65) Nelsen, S. F.; Konradsson, A. E.; Weaver, M. N.; Telo, J. P. *J. Am. Chem. Soc.* **2003**, *125*, 12493−12501.
(66) Nelsen, S. F.; Weaver, M. N.; Zink, J. I.; Telo, J. P. *J. Am. Chem. Soc.* **2005**, *127*, 10611−10622.
(67) Marcus, R. A.; Sutin, N. *Biochim. Biophys. Acta* **1985**, *811*, 265−322.
(68) Gray, H. B.; Winkler, J. R. *Proc. Natl. Acad. Sci. U. S. A.* **2005**, *102*, 3534−3539.
(69) Wenger, O. S. *Acc. Chem. Res.* **2011**, *44*, 25−35.
(70) Weiss, E. A.; Ahrens, M. J.; Sinks, L. E.; Ratner, M. A.; Wasielewski, M. R. *J. Am. Chem. Soc.* **2004**, *126*, 9510−9511.
(71) Hankache, J.; Wenger, O. S. *Chem.—Eur. J.* **2012**, DOI: 10.1002/chem.201200199.
(72) Krejčik, M.; Daněk, M.; Hartl, F. *J. Electroanal. Chem.* **1991**, *317*, 179−187.
(73) Tkachenko, N. V.; Rantala, L.; Tauber, A. Y.; Helaja, J.; Hynninen, P. H.; Lemmetyinen, H. *J. Am. Chem. Soc.* **1999**, *121*, 9378−9387.
(74) Hankache, J.; Hanss, D.; Wenger, O. S. *J. Phys. Chem. A* **2012**, *116*, 3347−3358.